> JSTQE-CON-BP2019-07475-2018 <

Application of scan-less two-dimensional confocal microscopy based on a combination of confocal slit with wavelength/space conversion

Eiji Hase, Takeo Minamikawa, Shuji Miyamoto, Yasuhiro Mizutani, Tetsuo Iwata,

Hirotsugu Yamamoto, and Takeshi Yasui

***Abstract*—Confocal laser microscope (CLM) has been widely used in the fields of the non-contact surface topography, biomedical imaging, and other applications, because the confocality gives two-dimensional (2D) optical-sectioning or three-dimensional (3D) imaging capability with the depth selectivity. Combination of line-focused CLM with one-dimensional (1D) spectral encoding CLM enables us to obtain the 2D confocal image without the need for the mechanical scanning. So-called scan-less 2D CLM is a unique imaging modality, however, there are no attempts to apply for practical application. In this paper, we constructed scan-less 2D CLM with the image acquisition time of 0.23 ms, the lateral resolution of 1.2 μm, the depth resolution of 2.4 μm, and apply it for different kinds of application to evaluate its practical potential.**

***Index Terms*—Biomedical imaging, Microscopy.**

I. Introduction

CONFOCAL laser microscopy (CLM) [1] has been widely used in the field of biomedical imaging, non-contact surface topography, and other applications thanks to the benefit of the noninvasiveness, the optical sectioning capability, and the stray light elimination. Usual CLMs are based on a point-scanning measurement. This is because a pinhole for a point light-source, a focal point of the objective lens, and a pinhole before a detector must have a conjugate relationship to each other. Therefore, a two-dimensional (2D) image has to be acquired by a mechanical scanning of the focal point while maintaining the conjugate configuration. The mechanical scanning by a galvanometer mirror, polygon mirror, or MEMS (Micro Electro Mechanical System) mirror leads to the image acquisition rate of several to a few tens frames per seconds (fps) [2, 3, 4]. The combination of a Nipkow disk with a micro-lens array boosts the image acquisition rate up to 1000 fps [5,6]. However, these mechanical scanning systems are susceptible to environmental disturbances, such as mechanical or acoustic vibration. Requirement for the stable experimental condition, such as an optical table, often limit the application of CLM inside the lab. To widely expand its application fields outside the lab, the mechanical scanning must be omitted from CLM.

Line-field CLM [7] is a one interesting approach to eliminate the one-dimensional (1D) mechanical scanning. In this method, the laser beam is focused on a sample as a line beam, and the line beam reflected from a sample passes through a confocal slit before the detection. This slit gives the confocality for the whole line image, and then the reflected light is captured as the confocal 1D image in real time by a 1D imaging sensor (line sensor). However, this approach still needs additional mechanical scanning of the line beam across the line illumination. Another interesting approach is the use of 1D spectral encoding (1D-SE) CLM [8,9]. In 1D-SE CLM, a rainbow line beam is formed by a combination of a broadband-spectral light and a diffraction grating, and then are irradiated on the sample as the line beam of the rainbow spectrum. This result in an encoding of 1D image information onto the rainbow spectrum. Finally, the 1D image is decoded from the spectrum acquired by a multi-channel spectrometer without the mechanical scanning. However, as well as the line-field CLM, additional 1D mechanical scanning needs to acquire the 2D image.

If the line-field CLM and the 1D-SE CLM are orthogonally combined, 1D image information of each coordinates are individually and orthogonally developed in the 2D plane. By using the multi-channel spectrometer equipped with the 2D imaging sensor, the confocal 2D image can be decoded from a spectral line image, composed of 1D spatial dimension and 1D spectral dimension, without the need for any mechanical scanning. The image acquisition rate of this approach is limited by not the mechanical scanning but the frame rate of the 2D

E. Hase and S. Miyamoto were with the Graduate school of Advanced Technology and Science, Tokushima University, Tokushima 770-8506, Japan (email: hase@spring8.or.jp; shuujimiyamoto@gmail.com). T. Minamikawa, T. Iwata, and T. Yasui are with the Graduate school of Technology, Industrial and Social Sciences, Tokushima University, Tokushima 770-8506, Japan (email: minamikawa.takeo@tokushima-u.ac.jp; iwata@tokushima-u.ac.jp; yasui.takeshi@tokushima-u.ac.jp). Y. Mizutani is with the Graduate School of Engineering, Osaka University, Osaka 565-0871, Japan. (email: mizutani@mech.eng.osaka-u.ac.jp). H. Yamamoto is with the Center for Optical Research and Education, Utsunomiya University, Tochigi 321-8585, Japan (email: yamamoto@opt.utsunomiya-u.ac.jp). All authors are with JST, ERATO, MINOSHIMA Intelligent Optical Synthesizer Project, 2-1, Tokushima 770-8506, Japan. (*Corresponding author: Takeshi Yasui*)

imaging sensor, which is achieved up to Mfps in the state-of-art complementary metal oxide semiconductor (CMOS) camera.

Such scan-less 2D CLM has a high potential as CLM due to the fast image acquisition rate and the high robustness to the environmental disturbances [10]. However, its potential of confocal 3D or volume imaging has not been fully investigated from the viewpoint of practical applications. In this paper, we expand the scan-less 2D CLM into confocal 3D imaging by help of a piezoelectric-transducer (PZT) scanner for objective lens, and then apply it for three applications, namely biomedical imaging of tissue specimen, plant monitoring, and non-destructive inspection of electronic board.

II. Principle

Figure 1 shows a principle of operation for the scan-less 2D CLM based on a combination of line-field CLM with 1D-SE CLM. In this figure, while the optical axis is defined as a *Z* coordinate, the horizontal and vertical directions in the 2D plane normal to the optical axis are respectively corresponding to *X* and *Y* coordinates. The *X* and *Y* coordinates are used for each 1D imaging by 1D-SE and line-field CLMs, respectively. The circular beam shape of a broadband-spectral laser light is converted into a line shape along the *Y* coordinate by the beam-shaping optics, composed of a cylindrical lens and a lens. The wavelength disperser disperses each wavelength component at different angle along the *X* coordinate depending on the wavelength. This results in a formation of "vertical rainbow" composed of the same wavelength component along the *Y* coordinate and the different wavelength components along the *X* coordinate. After passing thorough an objective lens, the demagnified vertical rainbow is illuminated on a sample. This enables to encode the 2D information of the sample on the vertical rainbow at one-shot.

The back-reflected vertical rainbow from the sample inversely propagates the same optical components, and each wavelength component is spatially overlapped again. The resulting line-shape beam passes through a confocal slit for the confocality of the 1D image along the *Y* coordinate. Then, the spectral line image, or the spatio-spectral image, is measured as an image with the wavelength dimension along the *X* coordinate and the spatial dimension along the *Y* coordinate by a multi-channel spectrometer equipped with a 2D imaging sensor. Since this spatio-spectral image is corresponding to the demagnified vertical rainbow on the sample, the confocal 2D image of the sample can be decoded without the need for mechanical scanning system.

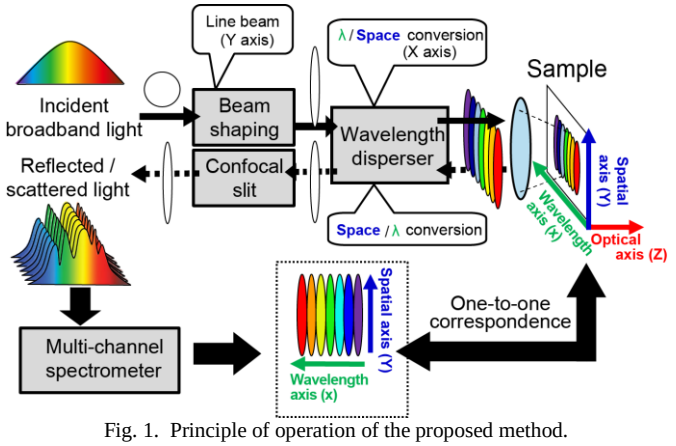

Fig. 1. Principle of operation of the proposed method.

III. Experimental Setup

Figure 2 shows a schematic diagram of the experimental setup. A broadband-spectral laser (Spectra-Physics, Inc., Santa Clara, CA, USA, InSight DeepSee, λ_C = 780 nm, $\Delta\lambda$ = 10 nm, P_{mean} = 900 mW) was used for the light source of scan-less 2D CLM. The output light was line-focused on a diffraction grating (G, Thorlabs, Inc., Newton, NJ, USA, GR25-1208, groove density = 1200 groove/mm, blaze wavelength = 750 nm) by a pair of a cylindrical lens (CL, f = 200 mm) and a lens (L1, f = 200 mm) after passing through a spatial filter and a beam expander (BE). The direction of the focused line on the grating was orthogonal to the groove direction. Each wavelength component of the light source was diffracted at different angles depending on the wavelength and then was focused on the sample by the combination of relay lenses (L2, f = 200 mm; L3, f = 200 mm) and the objective lens (OL, *NA* = 0.95, *Magnification* = 60). This results in the illumination of the vertical rainbow with a field of view (FOV) of 68 µm × 156.2 µm on the sample plane. Although the vertical rainbow is illustrated as a visible rainbow color for easy understanding, its actual color is considerably monochromatic in the near-infrared region. The reflected or scattered light at the sample inversely propagated the same optical path including the objective lens, the relay lenses, and the diffraction grating, leading to the inverse process of 1D-SE. Such the inverse 1D-SE process recovers the horizontally line-focused light on the grating again. After reflected by a beam splitter (BS), the horizontally line-focused light was converted as the vertically line-focused light and then passes through the incident slit of a multi-channeled spectrometer (Princeton instruments, Inc., Trenton, NJ, USA, Acton SP2300) equipped with a CMOS camera (Thorlabs, Inc., Newton, NJ, USA, DCC1545M, 1280×1024 pixels, pixel size = 5.2 µm square, bit depth = 10 bit, frame rate = 22 fps). The incident slit of the multi-channel spectrometer can be used for the confocal slit for the line-field CLM, too. Thus, the width of the incident slit determines not only the spectral resolution but

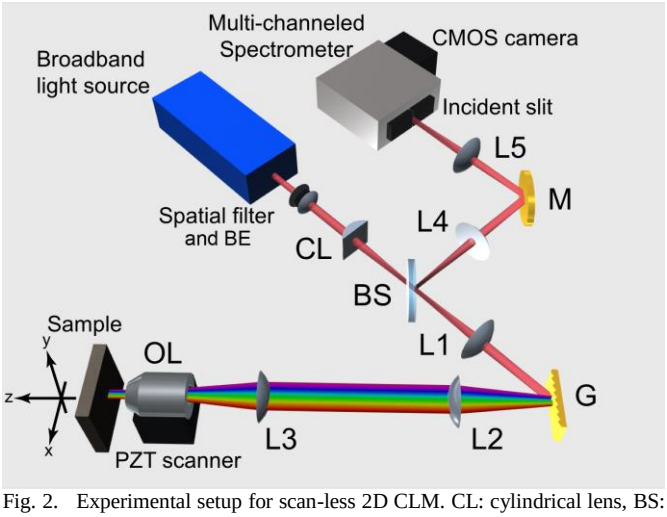

Fig. 2. Experimental setup for scan-less 2D CLM. CL: cylindrical lens, BS: beam splitter, G: grating, L: lens, OL: objective lens, M: mirror.

also the confocality for the *X* and *Z* coordinates. We here set the slit width to be 60 μm by taking into account of the central wavelength of the light source, the NA of the objective lens, and the magnification of the lens before the incident slit. This slit width is corresponding to the spectral resolution of 0.1 nm. In this way, the spectral line image was acquired by the spectrometer and the camera. Scanning the depth position of a sample with the PZT-driven OL scanner (Physik Instrumente, GmbH, Karlsruhe, Germany, P-721, travel range = 100 μm) enables us to acquire 3D confocal imaging of the sample.

IV. Results

A. *Imaging performance*

We first evaluated the lateral resolution for the *X* and *Y* coordinates in the constructed scan-less 2D CLM. A commercialized 1951 USAF resolution test chart with a negative pattern (Edmond Optics, Barrington, NJ, USA, #38-256) was placed at the focal position of the objective lens as a test sample. Figure 3(a) shows the confocal 2D image of the test chart (image size =156.2 μm × 68.0 μm, exposure time of CMOS camera = 0.23 ms) measured by the scan-less 2D CLM system. In this image, *X* and *Y* coordinates were corresponding to the line images obtained by 1D-SE CLM and the line-field CLM, respectively. The fringe pattern along the horizontal direction in Fig. 3(a) is due to the interference between the transmitted light and the multiple reflection light in the beam splitter. We extracted the amplitude profile across the pattern edge along a green line and a blue line in Fig. 3(a), and then calculated their differential curves [see green plots and blue plots in Figs. 3(b) and 3(c)]. These plots were considerably noisy due to the low signal-to-noise ratio (SNR). To reduce the influence of such nose in the profile, we first calculated the moving average of the differential curves in Figs. 3(b) and 3(c), and then performed the curve fitting analysis using a Gaussian function [see a green line and a blue line in Figs. 3(b) and 3(c)]. We here defined the lateral resolution in *X* and *Y* coordinates (δ_X and δ_Y) as a full width of half maximum (FWHM) for the differential curves of them. The resulting lateral resolution was determined to be 1.2 μm for δ_X and 1.2 μm for δ_Y. From the diffraction limit of light, theoretical δ_X and δ_Y values were given by [7,8,11]

$$\delta_X = 0.48\frac{\lambda}{NA} \quad (1)$$

$$\delta_Y = \frac{0.61\lambda}{NA} \quad (2)$$

where λ is a typical wavelength of light and *NA* is a numerical aperture of OL. Due to use of the confocal slit with the confocality along the *X* direction and without the confocality along the *Y* direction, the theoretical δ_X value was smaller than the theoretical δ_Y value. From λ = 780 nm and *NA* = 0.95 in the present system, theoretical δ_X and δ_Y values were estimated to 0.4 μm and 0.5 μm, respectively. We have to further consider the contribution of the spectral resolution in the spectrometer to the X lateral resolution because the X-line image is encoded on the optical spectrum in 1D-SE CLM. X dimension of FOV (= 156.2 μm) in Fig. 3(a) was corresponding to the spectral range of 773 nm to 788 nm with a spectral resolution of 0.1 nm. Therefore, the *X* lateral resolution determined by the spectral resolution, δ_{X_λ}, is estimated to be 0.5 μm. Since the theoretical δ_X value was larger than the δ_{X_λ} value, the former is a dominant factor of the X lateral resolution in the present system. In this way, the lateral resolution of the system is mainly determined by the diffraction limit in the same manner as usual optical microscopy. Difference of lateral resolution between the theoretical value and the experimental value is due to the imperfectly filling NA in the objective lens and/or the residual aberration.

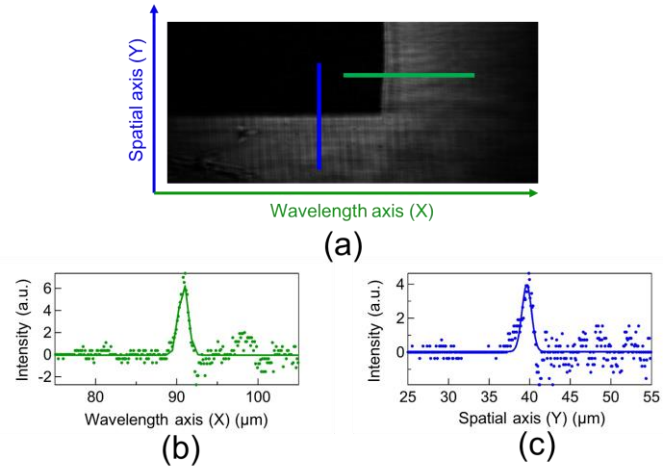

Fig. 3. (a) Scan-less 2D confocal image of the test chart (image size = 156.2 μm × 68.0 μm). Green and blue lines show the extracted portion for evaluation of the lateral resolution in X and Y directions. Differential curves of the extracted edge profile along (b) X direction and (c) Y direction. The plots indicate the experimental value, whereas the line indicate the curve fitting results with a Gaussian function.

We next evaluated the depth resolution δ_Z along *Z* coordinate. To this end, we measured the total signal intensity for 2 pixels by 2 pixels around the center of image when the *Z* position of the sample was moved at a step of 2 μm within the range of -18 μm to +18 μm. Red plots in Fig. 4 shows the depth profile of the signal intensity with respect to *Z* position. For comparison, the depth profile is indicated as green plots in the same graph when the confocal slit was fully opened. Comparison between them clearly indicated the sharp confocality along the depth direction. From the curve fitting analysis with a Gaussian function, the experimental δ_Z value was 2.4 μm from FWHM of the red depth profile. Let here us consider theoretical δ_Z value given by [7,8,11]

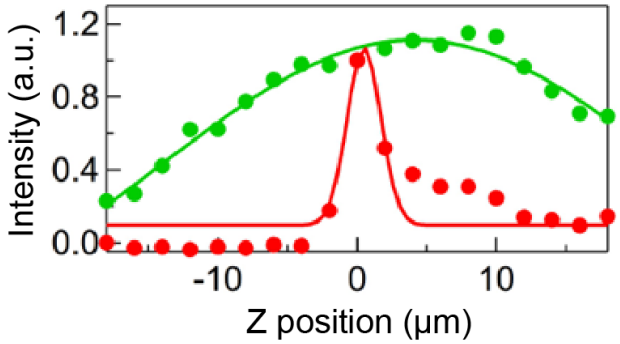

Fig. 4. Depth profile of scan-less 2D CLM. Red and green plots show the experimental depth profile with and without the confocal slit. Red and green lines indicate the corresponding to curve fitting results with a Gaussian function.

$$\delta_z = 0.88\frac{\lambda}{n - \sqrt{n^2 - NA^2}} \quad (3)$$

where n is a reflective index of the medium between OL and the sample. Substituting 780 nm for λ, 0.95 for NA, and 1 for n, we obtained δ_Z = 1.0 μm. Difference of depth resolution between the theoretical value and the experimental value is due to the imperfectly filling NA in the objective lens and/or the residual aberration similar to the lateral resolution.

We next performed depth-resolved confocal imaging, or volume imaging, of a standard sample with known dimension. to evaluate the imaging performance of the proposed system. We here used a transparent scotch tape (thickness ≈ 46 μm) as a standard sample with known thickness. To make a two-layered structure, two pieces of scotch tapes were attached orthogonally to each other at a slide glass as shown in Fig. 5(a). Movie 1 shows a series of depth-resolved 2D confocal images when the Z position of OL was scanned within the depth range of around 50 μm at 1.4 Hz. Figures 5(b) and 5(c) show two typical images (camera exposure time = 21 ms, frame rate = 18 fps) at different Z positions (Z = 0 μm and 45.1 μm), respectively. While the surface of the first-layer scotch tape was focused at Z = 0 μm, that of the second-layer scotch tape was focused at Z = 45.1 μm Difference of Z position between them was 45.1 μm, which is in good agreement with the specification of this tape. In this way, the depth-resolved confocal 2D image correctly reflects the 3D surface profile of the sample. The image contrast of the Figs. 5 (b) and (c) were sufficient to discriminate both layers of the transparent tape. Considering the high transparency in biological samples such as tissues and cells, this result implies that the proposed microscopy has a potential for 3D imaging of practical biomedical applications.

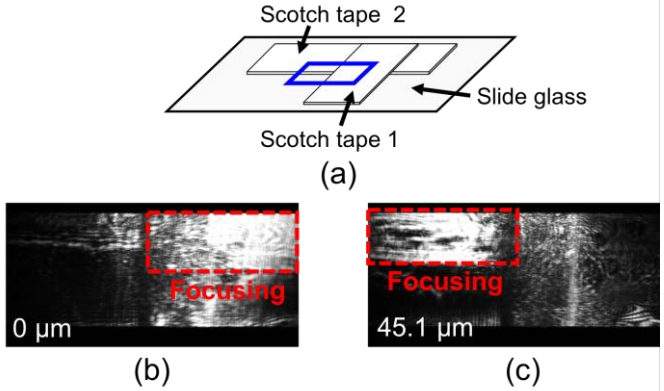

Fig. 5. Reflection imaging of the two-layered cellophane tape. (a) Schematic drawing of the two-layered cellophane tape. A blue rectangle is the measured portion. (b) Reflection image at objective position = 0 μm (c) Reflection image at objective position = 45.1 μm (image size = 156.2 μm × 68.0 μm).

B. *Observation of plant leaf*

Non-invasive observation of plant leaf is required for health monitoring of crops because dynamics of the plant leaf is closely related with the activity of living crops [12]. For example, stoma plays an important role to maintain internal environment by continuously exchanging gases with the atmosphere and diffusing water vapor through stoma for transpiration [13]. Therefore, opening and closing of stoma is a good indicator for the plant growth and health. One potential application of the scan-less 2D CLM is in an observation of plant leaf *in situ*. As a demonstration, we here used a tomato leaf as a plant sample. Figures 6(a) and 6(b) shows the optical photograph of the sample and its microscopic image (image size = 156.2 μm × 68.0 μm). Although the microscopic image was obtained by a normal optical microscope (*Magnification* = 20, *NA* = 0.42), it is difficult to observe the distribution of stomata in the tomato leaf due to the non-confocality. Figure 6(c) shows a sketch of leaf cross section. We here tried to acquire depth-resolved 2D confocal images from the side of upper epidermis. Movie 2 shows a series of depth-resolved 2D confocal images when the Z position of OL was scanned within the depth range of 40 μm at 0.5 Hz. Figure 6(d) shows three typical images at different Z positions (Z = 0 μm, 10 μm, and 30 μm). At Z = 0 μm, as the leaf surface was out of focus, no structure appeared in the image. At Z = 10 μm, while guard cells were focused as bright regions, the stoma appeared as a black region of vertical oval inside guard cells, indicating the stoma opening. At Z = 30 μm, upper epidermis and/or palisade mesophyll were visualized as compartments. In this way, scan-less 2D CLM enables us to visualize 3D structure of leaf plant with high contrast images in real time.

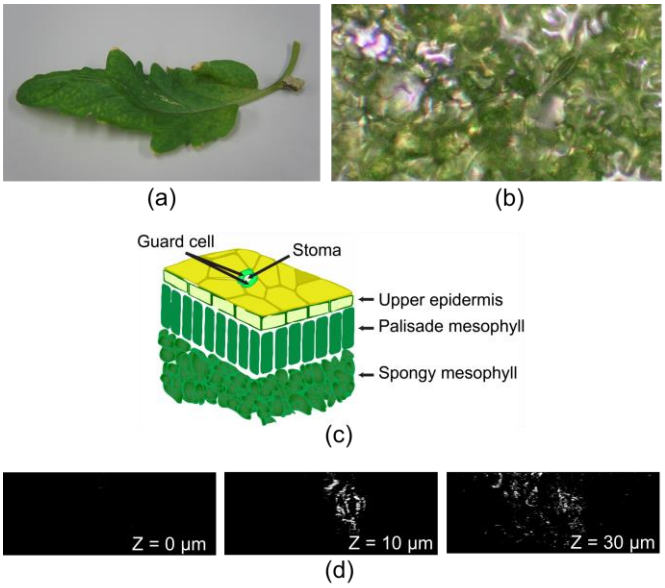

Fig. 6. (a) Optical photograph of a tomato leaf. (b) Microscopic image of the tomato leaf (*Magnification* = 20, *NA* = 0.42). (c) Sketch of the leaf cross section. (d) Depth-resolved 2D confocal images of the tomato leaf (image size = 156.2 μm × 68.0 μm).

C. *Imaging of biological tissue*

Staining method is a powerful tool in histopathology [14]. For the correct diagnosis with histopathology, a thin layer of lesion (typical thickness ≈ 5 μm) has to be appropriately extracted from a thick specimen of biopsy tissue before the staining. However, if a position of the sliced specimen is inappropriate, it might be the wrong diagnosis. Optical-sectioning imaging capability with the micrometer depth selectivity in the scan-less 2D CLM has a potential to find an application as a sample pre-processing tool in the histopathology.

To investigate a potential for such application, we demonstrated imaging of biological tissues. In this demonstration, to enlarge FOV, a lower-NA OL (*NA* = 0.25) was used for the scan-less 2D CLM. Using this system, δ_x of

13.9 μm, δ_Y of 2.4 μm, and δ_Z of 29.4 μm were achieved in the image size of 1.18 mm × 0.28 mm. Figure 7(a) shows the Hematoxylin-Eosin (HE) stained image of a sliced rat's skin sample (thickness = 5 μm). The enlarged view of the blue rectangle region in Fig. 7(a) is show in Fig. 7(b). The HE staining method enables the selective visualization of muscle tissue and extracellular matrix as pink color. In Fig. 7(b), muscle cells enveloped by fibrous connective tissue were clearly observed in the whole of image. We next measured the same sample by using the proposed method. Figures 7(c) and 7(d) show a comparison of the scan-less 2D image without and with confocal slit. While the tissue was visualized with some blur in Fig. 7(c) due to non-confocallty, Fig. 7(d) the enhances the image contrast due to the stray light elimination rather than the depth selectivity in the confocality. More importantly, the image quality in Fig. 7(b) is similar to that in Fig. 7(d); each unit of the muscle fiber bundles were clearly distinguished in the image.

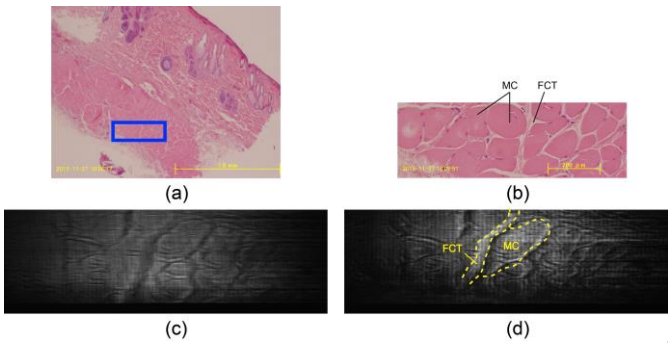

Fig. 7. (a) HE stained image of a rat's skin specimen. (b) Magnified image (image size = 0.84 mm × 0.28 mm) of a blue rectangle region in Fig. 7(a). MC; muscle cell, FCT; fibrous connective tissue. Scan-less 2D confocal images (image size = 1.18 mm × 0.28 mm) of the rat's skin (c) without and (d) with the confocal slit.

D. Non-destructive inspection of electric board

Finally, we measured an electric circuit board by the same lower-NA OL. as a demonstration for the non-destructive inspection in industrial filed. Figure 8(a) shows an optical photograph of the measured sample. The measured region was the electrode of the chip capacitor. We acquired a series of 2D confocal images (image size = 1.18 mm by 0.28 mm, exposure time = 9.15 ms, frame rate = 22 fps) when the sample position was axially scanned at a step of 50 μm from Z = -150 μm to Z = 900 μm. Figure 8(b) shows typical 2D confocal images at two different Z positions. At Z = -150 μm, no signal appeared due to out of focus for the sample. The image signal started to appear from Z = 0 μm, indicating the sample surface (not shown). The surface structure of the electrode of the chip capacitor was clearly observed with high image contrast at Z = 450 μm, whereas that of the electric board was observed at Z = 600 μm. We then reconstructed the volume image of this sample from a series of the depth-resolved 2D image. Figure 8(c) and Movie 3 show the reconstructed volume image, indicating the detailed 3D structure of the electric board. The total acquisition time of this volume image was 525 ms.

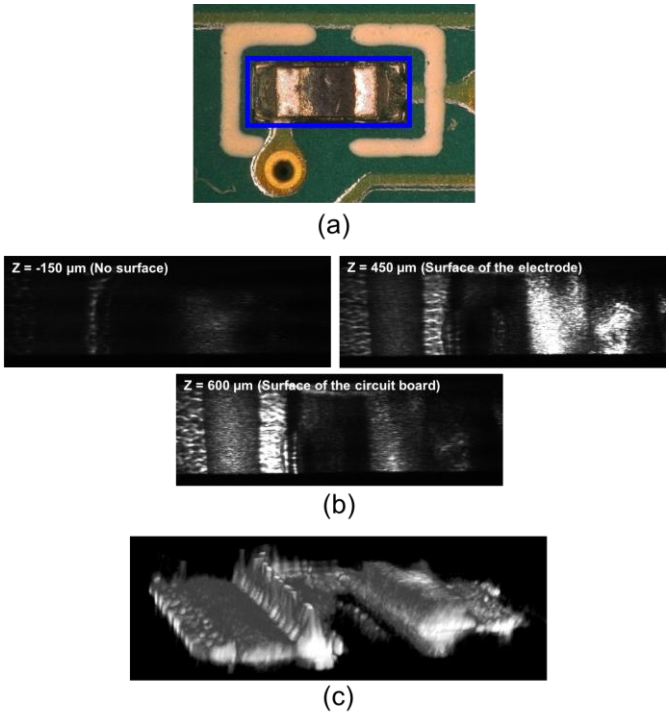

Fig. 8. (a) Optical photograph of an electric circuit board. The blue rectangle shows the measured region. (b) Depth-resolved scan-less 2D confocal images at z = -150, 450, and 600 μm. (c) 3D confocal image reconstructed by a series of depth-resolved scan-less 2D confocal images.

V. Discussion

We achieve the scan-less 2D CLM with the 0.23-ms acquisition time, the 1.2-μm lateral resolution, and the 2.4-μm depth resolution. We here compare this performance with that of the previous researches. Table 1 summarizes the imagining performance of the proposed method and other CLMs. There is no significant difference of lateral resolution and depth resolution among them because they depend on the diffraction limit of OL rather than the scanning method or the scan-less method. The two former methods have the confocality for X, Y, and Z axes while the three later methods have the confocality for X and Z axes; however, the lateral resolution for X and Y axes were almost similar to each other. Advantage or disadvantage of those methods are highlighted in the frame rate. Although the four former methods can achieve higher frame rate than the proposed method, the requirement for the mechanical scanning may hamper the practical application of CLM mentioned in the introduction. The frame rate of 2D image in the proposed method is limited by the camera frame rate, and the present frame rate remained at 22 fps by use of usual CMOS camera. However, one can use mega-fps CMOS camera now [15]. In other words, the proposed method has a potential to achieve mega-fps CLM. Such high frame rate cannot be achieved by other CLMs in principle. This comparison implies a high potential of the proposed system for practical CLM applications.

We next discuss the acquisition rate of volume imaging. In usual CLM, the acquisition rate is limited by the lateral scanning, the depth scanning, and/or the camera frame rate. Thanks to 2D scan-less capability based on a combination of the line-field CLM and the 1D-SE CLM, the present system

does not need the lateral scanning. The acquisition rate of the present system was limited by the PZT-driven OL scanner (scan rate ~ a few Hz) rather than the camera frame rate (= 22 fps). On the other hand, the moderate image contrast was obtained even with the exposure time of 0.23 ms [see Fig. 3(a)]. If a faster depth scanner and a higher-frame-rate camera are used for the scan-less 2D CLM, the acquisition rate of volume imaging will be further increased. Fortunately, there is still space to increase the scan rate of depth scanner and the frame rate of camera. For example, usual PZT-driven OL scanners have a resonant frequency of a few hundred Hz; use of a lightweight OL with the limited stroke will further increase its depth scan rate. Also, combination of OL with a focus-tunable lens will be useful for the fast depth scanning. Regarding the camera frame rate, the state-of-art CMOS camera can boost the frame rate up to 10^6 fps [15]. Use of these approaches enables us to achieve the video-rate volume imaging of moving objects with micrometer spatial resolution; this will find new applications not only in biomedical application but also industrial inspection.

Finally, we discuss expansibility of the proposed system for scan-less confocal fluorescent microscopy because the fluorescent microscopy is an important imaging modality in biomedical application. Unfortunately, the present system cannot be directly applied for the scan-less confocal fluorescent imaging because it depends on the one-to-one correspondence between the space and the wavelength. Conversion of the excitation light into the fluoresce by a sample cancels the spectral information and hence lose the one-to-one correspondence. However, use of wavelength sweeping light [16] or an intensity-modulated broadband-spectrum light [17] enables the scan-less confocal fluorescent imaging.

TABLE I
IMAGING FEATURE OF SEVERAL CLM APPROACHES

	Pont scanning	Area scanning (Nipkow)	Line-field	1D-SE	Proposed method
Confocal optics	Pinhole	Pinhole array	Slit	Slit	Slit
Confocality	X, Y, Z	X, Y, Z	X, Z	X, Z	X, Z
2D image acquisition	2D scanning	1D scanning	1D scanning	1D scanning	2D scan-less
Frame rate of 2D image	1 ~ 200 fps	1000 fps	191 fps	30 fps	22 fps (depending on camera)
Lateral resolution	X: 0.2 μm Y: 0.2 μm	X: 0.2 μm Y: 0.2 μm	X: 0.7 μm Y: 0.7 μm	X: 0.78 μm Y: no data	X: 1.2 μm Y: 1.2 μm
Depth resolution	0.3 μm	0.6 μm	3.3 μm	2.3 μm (theoretical)	Z: 2.4 μm
Reference	[1-4]	[5, 6]	[6]	[7, 8]	

VI. CONCLUSIONS

In this paper, we developed a scan-less 2D CLM by the combination of line-field CLM with the 1D-SE CLM, and further expanded it to 3D confocal imaging, or volume imaging, by help of a PZT-driven OL scanner. After the evaluation of the imaging performance, we provided a proof-of-principle demonstration for three potential applications. These demonstrations imply a high potential of the proposed system for these practical applications. If the scan-less 2D CLM can be integrated as a hand-held or endoscope CLM by help of a compact light source (e.g. LED or SLD) and fiber optics, its robust and simple characteristics will find the clinical applications including the intraoperative diagnosis.

ACKNOWLEDGMENT

This work a was supported by grants for the Exploratory Research for Advanced Technology (ERATO) MINOSHIMA Intelligent Optical Synthesizer (IOS) Project (JPMJER1304) from the Japanese Science and Technology Agency and a Grant-in-Aid for Scientific Research (A) No. 15H02026 from the Ministry of Education, Culture, Sports, Science, and Technology of Japan.

REFERENCES

[1] P. Davidovits, and D. Egger, "Scanning Laser Microscope," *Nature*, vol. 223, no. 5208, pp. 831, Aug. 1969.
[2] S. W. Paddock, "Confocal laser scanning microscopy," *BioTechniques*, vol. 27, no. 5, pp. 992-996, Nov. 1999.
[3] S. Choi, P. Kim, R. Boutilier, M. Y. Kim, Y. J. Lee, and H. Lee, "Development of a high speed laser scanning confocal microscope with an acquisition rate up to 200 frames per second," *Opt. Express*, vol. 21, no. 20, pp. 23611-23618, Oct. 2013.
[4] D. Lellouchi, F. Beaudoin, C. Le Touze, P. Perdu and R. Desplats, "IR confocal laser microscopy for MEMS Technological Evaluation," *Microelectron. Reliab.*, vol. 42, no. 9, pp. 1815-1817, Sep. 2002.
[5] T. Tanaami, S. Otsuki, N. Tomosada, Y. Kosugi, M. Shimizu, and H. Ishida, "High-speed 1-frame/ms scanning confocal microscope with a microlens and Nipkow disks," *Appl. Opt.*, vol. 41, no. 22, pp. 4704-4708, Aug. 2002.
[6] T. Shimozawa, K. Yamagata, T. Kondo, S. Hayashi, A. Shitamukai, D. Konno, F. Matsuzaki, J. Takayama, S. Onami, H. Nakayama, Y. Kosugi, T. M. Watanabe, K. Fujita, and Y. Mimori-Kiyosuea, "Improving spinning disk confocal microscopy by preventing pinhole cross-talk for intravital imaging", *Proc. Natl. Acad. Sci.*, vol. 110, no. 15, pp. 6241, Nov. 2012.
[7] K. B. Im, S. Han, H. Park, D. Kim, and B. M. Kim, "Simple high-speed confocal line-scanning microscope," *Opt. Express*, vol. 13, no. 13, pp. 5151-5156, Jun. 2005.
[8] G. J. Tearney, R. H. Webb, and B. E. Bouma, "Spectrally encoded confocal microscopy," *Opt. Lett.*, vol. 23, no. 15, pp.1152-1154, Aug. 1998.
[9] D. Yelin, I. Rizvi, W. M. White, J. T. Motz, T. Hasan, B. E. Bouma & G. J. Tearney, "Three-dimensional miniature endoscopy," *Nature*, vol. 443, no. 7113, pp. 765, Oct. 2006.
[10] J. Kim, D. Kang, and D. Gweon, "Spectrally encoded slit confocal microscopy," *Opt. Lett.*, vol. 31, no. 11, pp. 1687-1689, Jun. 2006.
[11] C. J. Sheppard and D. M. Shotton, "Performance of confocal microscopes," *Confocal Laser Scanning Microscopy*, 1st ed., Oxford, UK: BIOS Scientific Publishers, 1997, pp. 33-44.
[12] A. Méndez-Vilas, "In situ microscopic investigation of plant cell walls deconstruction in biorefinery," *Microscopy: advances in scientific research and education*, vol. 2, Badajoz, Spain: Formatex Research Center, 2014, pp. 426-433.
[13] G. D. Farquhar, and T. D. Sharkey, "Stomatal Conductance and Photosynthesis," *Annu. Rev. Plant Physiol.*, vol. 33, pp. 317-345, Jun. 1982.
[14] M. H. Ross, *Histology*, 5th ed., Philadelphia, PA, USA: LW&W, 2006.
[15] C. T. Chin, C. Lancée, J. Borsboom, F. Mastik, M. E. Frijlink, and N. de Jong, "Brandaris 128: A digital 25 million frames per second camera with 128 highly sensitive frames," *Rev. Sci. Instrum.*, vol. 74, no. 12, pp. 5026-5034, Dec 2003.
[16] M. Strupler, E. D. Montigny, D. Morneau, and C. Boudoux, "Rapid spectrally encoded fluorescence imaging using a wavelength-swept source," *Opt. Lett.*, vol. 35, no. 11, pp. 1737-1739, Jun. 2010.
[17] J. T. Motz, D. Yelin, B. J. Vakoc, and B. E. Bouma, "Spectral- and frequency-encoded fluorescence imaging," *Opt. Lett.*, vol. 30, no. 20, pp. 2760-2762, Oct. 2005.

Eiji Hase was born in Tokushima, Japan, in 1989. He received the B.S., M.S. and Ph.D. degrees in engineering from Tokushima University, Tokushima, Japan, in 2012, 2014 and 2017.

From 2014 to 2017, he was a Research Associate with the JST, ERATO, MINOSHIMA Intelligent Optical Synthesizer Project. Since 2017, he has been a Research Scientist with the Research and Utilization Division, Japan Synchrotron Radiation Research Institute, Sayo, Japan, and a Visiting Associate Professor with the Graduate School of Technology, Industrial and Social Sciences, Tokushima University. His research interests include Biomedical imaging and Biomechanical analysis using femtosecond laser and synchrotron X-ray.

Dr. Hase was a recipient of The Optical Society of Japan Best Presentation Award in 2016, The Japanese Society for Medical and Biological Engineering Symposium Award in 2016, The International Society for Optical Engineering (SPIE) BiOS2016 in Photonics West 2016 Student Poster Awards in 2016, and SPIE Structured light 2018 Best Paper Award. He is a member of SPIE.

Takeo Minamikawa was born in Ibaraki, Japan, in 1983. He received the B.S., M.S. and Ph.D. degrees in engineering from Osaka University, Osaka, Japan, in 2006, 2008 and 2010.

From 2010 to 2013, he was a Research Fellowship for Young Scientists with Japan Society for the Promotion of Science. From 2013 to 2015, he was an Assistant Professor with Department of Pathology and Cell Regulation, Graduate School of Medical Science, Kyoto Prefectural University of Medicine. Since 2015, he has been an Associate Professor with Department of Mechanical Science, Division of Science and Technology, Graduate School of Technology, Industrial and Social Sciences, Tokushima University, Tokushima, Japan. He is the author of two book chapters, more than 30 articles, and more than 15 inventions. His research interests include Raman microspectroscopy and optical-frequency-comb. He holds three patents.

Dr. Minamikawa's awards and honors include The Japan Society for Precision Engineering Best Presentation Award in 2016, The Japanese Society of Pathology Poster Presentation Award in 2015, and Funai Foundation for Information Technology Research Award in 2011. He is a member of the Optical Society of America (OSA), the Japan Society of Applied Physics, the Optical Society of Japan, the Laser Society of Japan, the Japan Society of Mechanical Engineers, the Japan Society for Precision Engineering.

Shuji Miyamoto was born in Tokushima, Japan, in 1992. He received the B.S., M.S. degree in mechanical engineering from Tokushima University, Tokushima, Japan, in 2015, 2017. From 2014 to 2017, he studied about Nonlinear Optics under Prof. Takeshi Yasui, Tokushima University. His research was about Dual-optical-comb spectroscopy and Scan-less confocal microscope using broadband light source. From 2017, he has been an Engineer with the SCREEN Semiconductor Solutions Company Limited, Shiga, Japan.

Mr. Miyamoto was a recipient of The Japanese Society for Medical and Biological Engineering Branch Conference Young Researcher Award in 2016.

Yasuhiro Mizutani obtained his Ph.D. degree in mechanical engineering from Tokyo university of Agriculture & Technology, Tokyo, Japan, in 2008. He has also BE and ME degrees in nuclear engineering form Osaka university in 1997 and 1999, respectively.

From 1999 to 2003, he joined as a researcher at Panasonic Corporation. Then, from 2003 to 2009, he worked as a research associate in the Department of Mechanical systems engineering at Tokyo university of Agriculture & Technology, Japan. He joined the University of Tokushima, Japan, in 2009 as an associate professor. He is currently an associate professor at Osaka university from 2015.

Prof. Mizutani's research interests include interferometry, polarimetry, 3D surface measurement, optical trapping, and 3D lithography. In these areas, he has published over 100 papers in refereed international journals and conferences. He is a member of SPIE and OSA.

Tetsuo Iwata received the Ph.D. degree in engineering from Osaka University, Osaka, Japan, in 1984.

From 1984 to 1998, he worked in JASCO Corporation, Japan. He is currently a Professor in the Graduate School of Technology, Industrial and Social Sciences, Tokushima University, Tokushima, Japan.

Prof. Iwata's research interests include Fluorescent measurement and spectroscopy.

Hirotsugu Yamamoto received the Ph.D. degree in information science and technology from the University of Tokyo, Tokyo, Japan, in 2008.

From 1996 to 2014, he worked in Tokushima University, Japan. He is currently an Associate Professor in the Graduate School of Engineering, Utsunomiya University, Utsunomiya, Japan.

Prof. Yamamoto's research interests include Information optics.

Takeshi Yasui received the first Ph.D. degree in engineering from the University of Tokushima, Tokushima, Japan, in 1997, and the second Ph.D. degree in medical science from the Nara Medical University, Yagi, Japan, in 2013.

From 1997 to 1999, he worked as a Post-Doctoral Research Fellow in the National Research Laboratory of Metrology, Japan. He was with the Graduate School of Engineering Science, Osaka University from 1999 to 2010, and was briefly with the University of Bordeaux I in 2007 and 2012, and with the University of Littoral Côted'Opale in 2010 as an Invited Professor. He is currently a Professor in the Graduate School of Technology, Industrial and Social Sciences, Tokushima University, Tokushima, Japan, Vice Director of Research Support in the same university since 2016, and an Invited Professor in the Graduate School of Engineering Science, Osaka University, Toyonaka, Japan. His research interests include THz instrumentation and metrology, second-harmonic-generation microscopy, and optical frequency comb.

Prof. Yasui is a member of the Optical Society (OSA), The International Society for Optical Engineering (SPIE), the Japan Society of Applied Physics, the Optical Society of Japan, the Laser Society of Japan, the Japanese Society for Medical and Biological Engineering, and the Japan Society of Mechanical Engineers. He received the Award for the Most Promising Young Scientist from the Optical Society of Japan in 1998, the Sakamoto Award from the Japan Society of Medical Electronics and Biological Engineering in 2006, the Optics Paper Award from the Japan Society of Applied Physics, and the Funai Award from the Japan Society of Mechanical Engineers in 2009, the Original Paper Award from the Laser Society of Japan in 2013.